The Astrophysical Journal, 572:897–905, 2002 June 20
© 2002. The American Astronomical Society. All rights reserved. Printed in U.S.A.

ASCA OBSERVATIONS OF THE SUPERNOVA REMNANT IC 443: THERMAL STRUCTURE AND DETECTION OF OVERIONIZED PLASMA

Masahiro T. Kawasaki,[1] Masanobu Ozaki,[1] Fumiaki Nagase,[1] Kuniaki Masai,[2] Manabu Ishida,[2] and Robert Petre[3]

Received 2001 November 21; accepted 2002 February 22

ABSTRACT

We present the results of X-ray spatial and spectral studies of the "mixed-morphology" supernova remnant IC 443 using *ASCA*. IC 443 has a center-filled image in the X-ray band, contrasting with the shell-like appearance in radio and optical bands. The overall X-ray emission is thermal, not from a synchrotron nebula. We observed IC 443 three times with *ASCA*, covering the whole remnant. From the image analysis, we find that the softness-ratio map reveals a shell-like structure. At the same time, its spectra require two (1.0 and 0.2 keV) plasma components; the emission of the 0.2 keV plasma is stronger in the region near the shell than in the center. These results can be explained by a simple model that IC 443 has a hot (1.0 keV) interior surrounded by a cool (0.2 keV) outer shell. From the emission measures, we infer that the 0.2 keV plasma is denser than the 1.0 keV plasma, suggesting pressure equilibrium between the two. In addition, we find that the ionization temperature of sulfur, obtained from the H-like to He-like Kα intensity ratio, is 1.5 keV, significantly higher than the gas temperature of 1.0 keV suggested from the continuum spectrum. The same can be concluded for silicon. Neither an additional, hotter plasma component nor a multitemperature plasma successfully account for this ratio, and we conclude that the 1.0 keV plasma is overionized. This is the first time that overionized gas has been detected in a supernova remnant (SNR). For the gas to become overionized in the absence of a photoionizing flux, it must cool faster than the ions recombine. Thermal conduction from the 1.0 keV plasma to the 0.2 keV plasma could cause the 1.0 keV plasma to become overionized, which is plausible within an old (3×10^4 yr) SNR.

Subject headings: conduction — ISM: individual (IC 443) — plasmas — radiation mechanisms: thermal — supernova remnants

1. INTRODUCTION

Supernova remnants (SNRs) have been traditionally classified into three categories: shell-like, Crab-like (plerionic; its emission mainly originates from a pulsar nebula), and composite (shell-like containing a plerion). These SNRs usually have similar X-ray and radio morphologies. In addition to these, there is a recently established class characterized by a center-filled morphology and thermal emission in the X-ray band, contrasting with a shell-like structure in the radio and optical bands. Rho & Petre (1998) termed these "mixed-morphology" SNRs (MM SNRs). The distinctive characteristics of this category are that (1) the dominant X-ray emission mechanism is thermal despite an X-ray morphology similar to Crab-like SNRs; (2) the emission arises primarily from the swept-up interstellar material (ISM), not from ejecta; and (3) they are usually near or interacting with molecular clouds or other large ISM structures.

Rho & Petre (1998) identified two formation mechanisms that might explain the properties of MM SNRs. One is the cloud evaporation model, in which the interior X-ray emission arises from the gas evaporated from shocked clouds (White & Long 1991). For this model to match the properties of MM SNRs, the clouds must be numerous, small in size, and of sufficient density to survive in the passage of a strong shock. They pass into the hot interior of the remnant, gradually evaporating and emitting X-rays. The other is the thermal conduction model (Cox et al. 1999; Shelton et al. 1999). In this model, the shell of an expanding SNR cools below $\sim 10^6$ K, and its X-ray emission becomes too soft to be detected through the absorbing ISM. The thermal energy stored in the shocked interior gas is conducted outward, producing the observed uniform interior temperatures. This model requires sufficient interior density for conduction to be viable.

IC 443 (G189.1+3.0) is one of the prototypical MM SNRs. It has a $\sim 45'$ diameter and is located at a distance of 1.5 kpc (Fesen 1984). It is strongly interacting with a foreground molecular cloud and an H I cloud to the east (Cornett, Chin, & Knapp 1977; Giovanelli & Haynes 1979). It is a candidate for the *Compton Gamma Ray Observatory* (*CGRO*) EGRET γ-ray source 3EG J0617+2238 (Hartman et al. 1999). Its X-ray morphology was observed by *Einstein* to be center-filled, which is highly atypical of an SNR in the adiabatic phase, with little correlation with the radio or optical image. The spectrum of the brightest area was well described by either a 1.5 keV nonequilibrium ionization (NEI) plasma or 0.2 and 0.95 keV ionization equilibrium plasma components (Petre et al. 1988). Asaoka & Aschenbach (1994) analyzed *ROSAT* all-sky survey and pointing data and found another partially overlapping SNR of $\sim 10^5$ yr age, which they called G189.6+3.3. They reproduced the spectra for the regions excluding the part overlapping with G189.6+3.3 by a two-temperature (1 and $\sim$0.3 keV) ionization equilibrium plasma model.

[1] Institute of Space and Astronautical Science, 3-1-1 Yoshinodai, Sagamihara, Kanagawa 229-8510, Japan; kawasaki@astro.isas.ac.jp, ozaki@astro.isas.ac.jp, nagase@astro.isas.ac.jp.

[2] Department of Physics, Tokyo Metropolitan University, Hachioji, Tokyo 192-0397, Japan; masai@phys.metro-u.ac.jp, ishida@phys.metro-u.ac.jp.

[3] Laboratory of High Energy Astrophysics, Code 662, NASA/Goddard Space Flight Center, Greenbelt, MD 20771; rob@lheapop.gsfc.nasa.gov.

Using *Ginga*, Wang et al. (1992) found a hard X-ray component in the spectrum of IC 443 extending up to 20 keV. They suggested that this component originates from a very high temperature ($\gtrsim 10^8$ K) plasma and thus that the remnant's age is about 10^3 yr, instead of the previous estimate of 10^4 yr. However, *ASCA* and *BeppoSAX* revealed that this hard component is nonthermal and originates in two small regions along the southern edge of the radio shell, where the SNR–molecular cloud interaction is strongest (Keohane et al. 1997; Bocchino & Bykov 2000). Using *Chandra* data, Olbert et al. (2001) determined that one of the regions is a synchrotron nebula powered by a compact source (probably a neutron star), whose kick velocity is consistent with an age of 3×10^4 yr.

In this paper, we first present the *ASCA* Gas Imaging Spectrometer (GIS) images and softness-ratio map (§ 3.1). This reveals the existence of a soft, shell-like structure. We compare the Solid-State Imaging Spectrometer (SIS) spectra of the north region near the shell with that of the central region (§ 3.2) and then perform the spectral fitting (§ 3.3). Finally, we discuss a possible mechanism that can account for our results for the ionization state of IC 443 (§ 4).

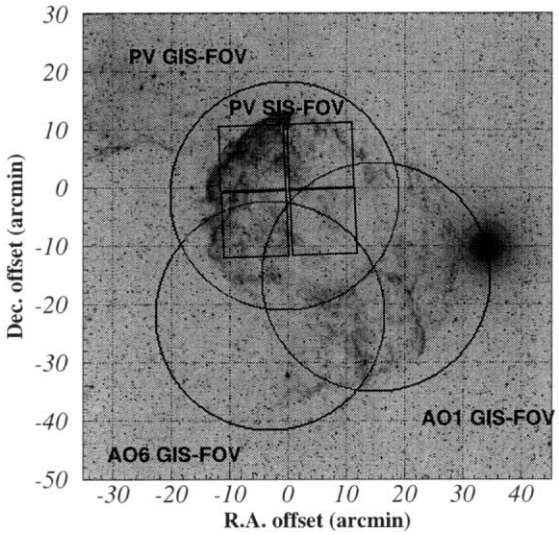

FIG. 1.—Fields of view of *ASCA* GIS and SIS used in the current analysis of IC 443 (20′ radius region for GIS and whole SIS field of view), superposed on the Palomar Observatory Sky Survey red image. Offsets indicated are in arcminutes relative to the adopted center at R.A. = $06^h17^m20^s$, decl. = 22°40′50″ (J2000.0).

2. OBSERVATIONS

ASCA has two solid-state imaging spectrometers (SIS 0, SIS 1) and gas imaging spectrometers (GIS 2, GIS 3) at the focal planes of the X-ray telescopes (XRTs). For IC 443, three observations were carried out. Figure 1 shows the fields of view (FOVs) of the observations in the current analysis (20′ radius region in the GIS and entire SIS FOV) superposed on the Palomar Observatory Sky Survey red image. The relevant information about these observations is given in Table 1. We extracted these data from the *ASCA* public archive. We used all available GIS data. During the AO-1 phase, the GIS 3 pulse-height analyzer (PHA) suffered from an onboard processing problem: the least significant PHA bits were stuck, resulting in a loss of spectral resolution. Therefore, the GIS 3 AO-1 data used here have only eight binned PHA channels. For the SIS, we used only the performance-verification (PV) phase observation data. There are enough photons from this observation to allow investigation of the spatial variation of the X-ray spectra with good energy resolution.

For the most part, the NASA Goddard Space Flight Center revision 2 standard data processing criteria were used for screening all the GIS and SIS data. The lone exception was for the earth elevation angle for the SIS: in order to avoid contamination by stray light, we used only data taken at angles more than 20°. Since the PV phase SIS data show no radiation damage effects, we did not apply the residual dark distribution correction.

As IC 443 is located in the Galactic anticenter region $(l, b) = (189.^\circ1, 3.^\circ0)$, where the Galactic ridge emission is negligible, we used blank-sky data that included the cosmic X-ray background (CXB) and the non–X-ray background (NXB) for background subtraction. The PV phase GIS data, with no spread discriminator application, contain more NXB events than those in subsequent observations. For these data, we used the background data sets that are applicable to observations performed when the GIS spread discriminator was turned off.

TABLE 1
ASCA OBSERVATION LOGS OF IC 443

PARAMETER	OBSERVATION PHASE		
	PV	AO-1	AO-6
Sequence Number	10011010, 10011020	51023000	56057000
R.A. (J2000.0)	06 17 26	06 17 18	06 17 34
Decl. (J2000.0)	22 40 48	22 26 45	22 20 22
Date	1993 Apr 14–15	1994 Mar 9–10	1998 Mar 25–27
Observation mode: SIS	4 CCD	4 CCD	2 CCD
Observation mode: GIS	Standard-PH	Standard-PH	Standard-PH
Effective exposure time: SIS 0 (ks)	35.4	...	...
Effective exposure time: SIS 1 (ks)	36.6	...	...
Effective exposure time: GIS 2 (ks)	39.7	35.4	37.5
Effective exposure time: GIS 3 (ks)	39.7	35.4	37.5

NOTE.—Units of right ascension are hours, minutes, and seconds, and units of declination are degrees, arcminutes, and arcseconds.

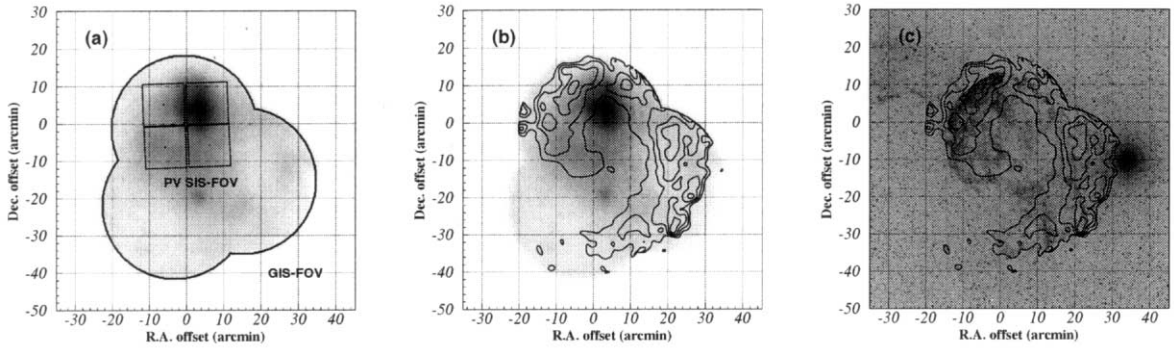

FIG. 2.—(*a*) Vignetting- and exposure-corrected GIS 0.7–10.0 keV band image with both SIS and GIS FOV boundaries. GIS softness-ratio ($F_{0.7-1.5\,\mathrm{keV}}/F_{1.5-10.0\,\mathrm{keV}}$) contours are shown over (*b*) the GIS 0.7–10.0 keV band image and (*c*) the Palomar Digital Sky Survey image. The scale of softness-ratio contours is linear, and their levels are 60%, 70%, 80%, and 90% of the peak value. Gray scales of the GIS and sky-survey images are linear and log, respectively. The offset center of each figure is R.A. = $06^{\mathrm{h}}17^{\mathrm{m}}20^{\mathrm{s}}$, decl. = $22^{\circ}40'52''$. The contours are limited at the FOV edge of the GIS along the northwest boundary, indicating that the remnant extends farther. The spotlike structure seen at (2, −20) in the GIS image is the so-called nonthermal component HXF (Keohane et al. 1997; Bocchino & Bykov 2000; Olbert et al. 2001).

In the present analysis, we used DISPLAY45, Version 1.90 for the image analysis and XSPEC, Version 11.0 for the spectral analysis.

3. DATA ANALYSIS AND RESULTS

3.1. *Image Analysis*

We generated a complete image of IC 443 using GIS data. The three GIS 2 and GIS 3 images were superposed, and an exposure-corrected blank-sky image was subtracted from it. We multiplied the simulated XRT efficiency map by the GIS grid map to form the vignetting image. Each map was smoothed by the corresponding point-spread function (PSF). We constructed the exposure-corrected vignetting image and divided it into the source image to create a vignetting- and exposure-corrected composite image. Figure 2*a* shows the resulting GIS image in the 0.7–10.0 keV band with *ASCA* FOVs.

In every energy band, the composite image shows IC 443 to have a center-filled morphology. The remnant is larger in images below 1.5 keV than in higher energy bands. Thus, a softness-ratio ($F_{0.7-1.5\,\mathrm{keV}}/F_{1.5-10.0\,\mathrm{keV}}$) map reveals a shell-like structure, contrasting with the center-filled appearance in the X-ray maps (see Fig. 2*b*). As shown in Figure 2*c*, the soft shell corresponds well with the bright optical emission in the northeast and southwest. The contours are limited at the FOV edge along the northwest boundary, indicating that it extends farther. The absence of the softness-ratio shell in the southeast and its low contrast in the northwest may be due to the absorption by the molecular cloud in front of IC 443 (Cornett et al. 1977).

In Figure 3 we show background-subtracted and exposure- and vignetting-corrected SIS images in the 0.5–1.0 keV and 1.0–2.0 keV bands. The SIS FOV includes both the brightest X-ray region of IC 443 and a part of the northeast shell. The peak surface brightness of the soft (0.5–1.0 keV) component appears to the north of that of the hard (1.0–2.0 keV) component (i.e., closer to the rim).

Therefore, both the GIS and SIS images suggest that a soft ($\lesssim$1.0 keV) X-ray component dominates near the shell, while a hard ($\gtrsim$1.5 keV) one dominates in the interior.

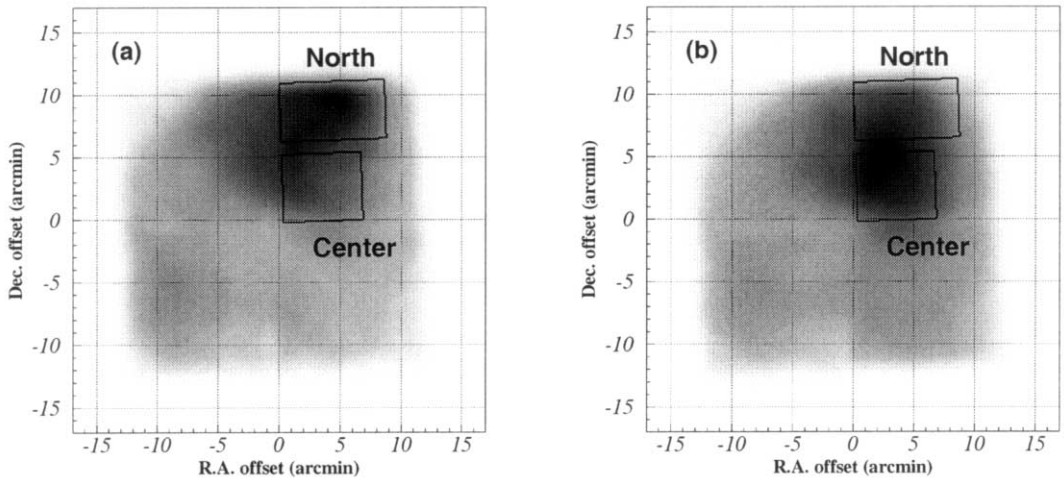

FIG. 3.—Exposure- and vignetting-corrected SIS images of (*a*) 0.5–1.0 keV and (*b*) 1.0–2.0 keV bands. The two boxes are spectra extraction regions named "north" and "center." The offset center of each figure is R.A. = $06^{\mathrm{h}}17^{\mathrm{m}}20^{\mathrm{s}}$, decl. = $22^{\circ}40'52''$.

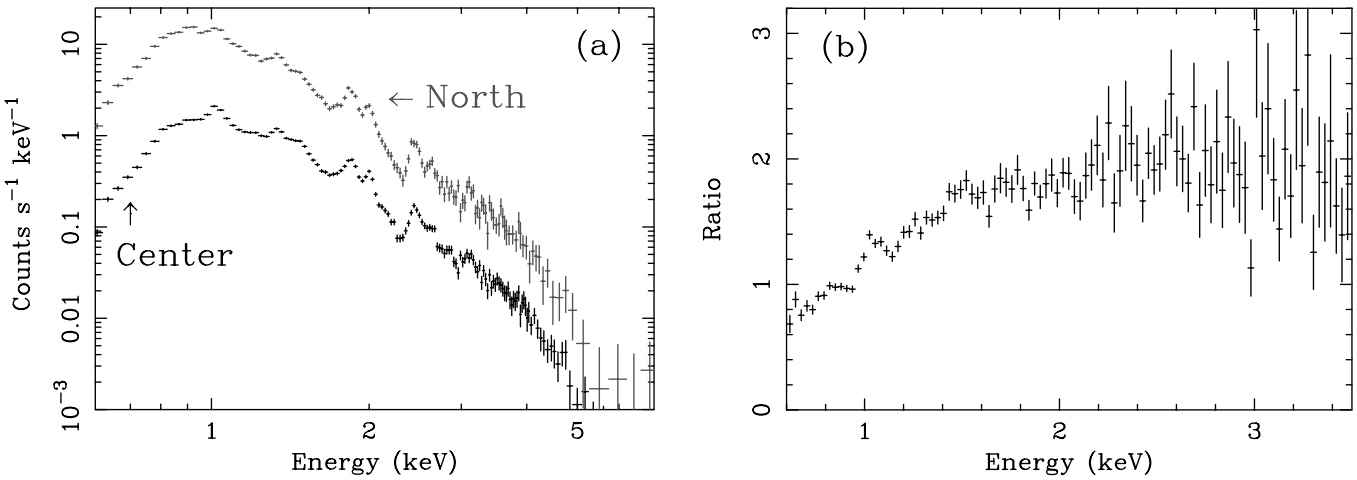

FIG. 4.—SIS spectra of the center and north regions. (*a*) Center and north spectra in black and gray, respectively. The spectrum of the north region is renormalized to 10 times the original. (*b*) Intensity ratio of center to north without any renormalization. Below 1.4 keV, the ratio decreases proportionally with energy.

3.2. *Difference between Two Regions*

We therefore searched for a spectral variation from the interior to the rim. We used only SIS data for the spectral analysis because the SIS has superior energy resolution to the GIS (FWHM of 5% at 1.5 keV during the observation; Tanaka, Inoue, & Holt 1994) and a larger effective area below 1 keV. We extracted spectra from the two regions indicated by boxes in Figure 3: a region near the northern rim (hereafter north) where the soft X-ray emission is stronger and an interior region (hereafter center) where the hard emission is stronger. Neither region overlaps G189.6+3.3, and stray light from the outside of the SIS FOV is negligible, as shown in Figure 2*a*. The spectra and their ratio are shown in Figure 4.

Above 1.4 keV, the shapes of the spectra appear similar to each other (see Fig. 4*b*) and are in good agreement with the spectrum from a thin thermal plasma with a temperature of about 1 keV. Below 1.4 keV, on the other hand, the north spectrum has relatively stronger emission than the center and shows the Ne IX emission line at 0.92 keV. The intensity ratio of the center spectrum to the north below 1.4 keV is proportional to the energy, as shown in Figure 4*b*. This ratio would be an exponential function of energy if the difference were due to higher column density. Therefore, it is difficult to explain this difference as a result of column density variation.

3.3. *Spectral Analysis*

In order to characterize the spectral properties and evaluate the difference between the two regions quantitatively, we performed model fittings; first with a one-component plasma model and then with a two-component plasma model. Since the SIS quantum efficiency changes greatly at the energy of the oxygen edge (0.53 keV), we did not use the data below 0.6 keV.

3.3.1. *One-Component Plasma Model*

We first applied a simple single-temperature, single ionization timescale, NEI plasma model (NEI in XSPEC; Borkowski 2000) that was favored in the previous IC 443 analysis (Petre et al. 1988). However, the minimum values of reduced χ^2 were 924/118 for the north and 1337/128 for the center, even with variable abundances, which are hardly acceptable.

We therefore tried an ad hoc model consisting of thermal bremsstrahlung, plus 12 Gaussian profiles to represent the most prominent emission lines above 0.9 keV. The line widths and strengths were all left free. Such models have been used previously to model *ASCA* spectra for other remnants (e.g., Miyata et al. 1994; Holt et al. 1994). Both H-like and He-like Kα lines of Mg, Si, and S were well fitted with negligible line widths compared to the energy resolution of the SIS.

The flux of each Gaussian profile is proportional to the emissivity of the line component. The line intensity ratio of H-like to He-like Kα (hereafter $R_{\rm H/He}$) provides a measure of the degree of ionization of a given element and depends on both the electron temperature and the ionization timescale. We evaluated the $R_{\rm H/He}$ for Mg, Si, and S through comparison with the theoretical values (Mewe, Gronenschild, & van den Oord 1985), as shown in Figure 5, and

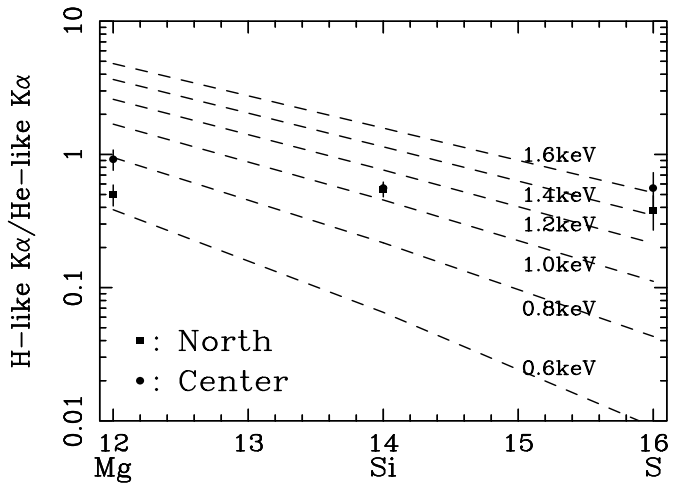

FIG. 5.—Ratios of the fitted Gaussian fluxes of H-like to He-like Kα for Mg, Si, and S. Filled squares and circles show data from the north and center, respectively. This ratio represents the ionization degree of each element. The dashed line represents the ratios of H-like to He-like Kα with each ionization temperature calculated based on Mewe et al. (1985). All data are on different lines of ionization temperature.

found that it is impossible to explain the degree of ionization of all elements with the same ionization temperature in each region. This suggests that more than one plasma component is required.

3.3.2. *Two-Component Plasma Model*

We next applied a two-component plasma model. The continuum components above 1.4 keV of the two spectra have a shape consistent with a temperature of 1 keV, as mentioned previously. In addition, Si and S appear to be ionized enough to apply a collisional-ionization equilibrium (CIE) model at this temperature (see Fig. 5). We thus used the CIE plasma model (VRAYMOND in XSPEC; Raymond & Smith 1977) as the high-temperature plasma. On the other hand, we used the generalized NEI model with varying temperature (VGNEI in XSPEC; Borkowski 2000) as the low-temperature plasma. All abundances were treated as variables, and those of two components linked together. This model failed to reproduce the Kα lines of Ne x, Si XIV, and S XVI (and the Kβ line of Ne x in the center), so we added several narrow Gaussian components.

We were able to reasonably fit both north and center spectra (except for the energies around the emission lines of Si and S) with a model consisting of a $\sim$0.2 keV NEI and a $\sim$1.0 keV CIE plasma with a column density of 7.4×10^{21} cm^{-2}, as shown in Figure 6. The best-fit parameters of the model are listed in Table 2. All abundances are smaller than the solar values (Anders & Grevesse 1989), which suggests that the X-rays originate from the shocked ISM. Although these fits are not formally acceptable, the result implies that the spectrum can be generally described by two plasma components: Figure 6 suggests that the spectra below 1.4 keV are well reproduced by the low-temperature ($\sim$0.2 keV) plasma, whereas those above 1.4 keV show the features of the 1.0 keV plasma.

Almost all fitted parameters for the two spectra are consistent with each other within a 90% confidence range. This suggests that the plasma properties in the two regions are similar. The sole significant difference is the ratio of the emission measures of the 0.2 keV plasma to the 1.0 keV one: it is substantially higher in the north (185^{+102}_{-68}) than in the center (48^{+39}_{-24}). Hence, we suggest that the difference of the intensity ratio between the two plasma components produces the apparent difference of the spectra shown in Figure 4.

While the two-component model accounts reasonably well for the gross spectral features, it leaves an important detail unresolved. The H-like lines of Ne, Si, and S are so strong that it is necessary to add Gaussian components to represent them.

In order to investigate the anomalous S line ratio, we fit the 2.2–6.0 keV spectra with a model consisting of a CIE plasma and three narrow Gaussian components (S XV Kα, S XVI Kα, S XV Kβ). (We can ignore the contribution of the 0.2 keV plasma component at the energies around the S lines.) The fits are acceptable, as shown in Figure 7. The $R_{\rm H/He}$ for S requires an ionization temperature (hereafter T_z) of about 1.5 keV in each region, higher than the continuum temperature (hereafter T_e) of 1.0 keV, as shown in Figure 8. The same can be concluded for Si. Ne x emits mostly around $kT_e = 0.5$ keV, which might indicate that the strong Ne x line comes from an intermediate-temperature (0.2 keV $< kT_e <$ 1.0 keV) plasma.

To account for the higher ionization temperatures of Si and S, we replaced the Gaussians with a second, hotter (2.0 keV) CIE component, whose temperature is selected to maximize the emissivity of the H-like line of S. However, this component requires an extraordinarily large S abundance; more than 10^3 solar. Such a large abundance is not observed even in ejecta, and thus this model is physically implausible. Moreover, narrowband images at the energies corresponding to Si and S H-like Kα lines show no conspicuous (e.g., clumpy) structure and are similar to those of other bands (e.g., images for Si and S He-like Kα and continuum bands), indicating that the H-like lines are emitted from the same plasma that emits He-like lines.

Another possible source of the anomalous ratio between T_z and T_e is a temperature distribution in the plasma, as observed in magnetic cataclysmic variables (Ezuka & Ishida 1999). However, as in SNRs, such plasma shows $T_z < T_e$ and thus does not explain the higher T_z of Si and S. Therefore, we suggest that the Kα lines of H-like Si and S are

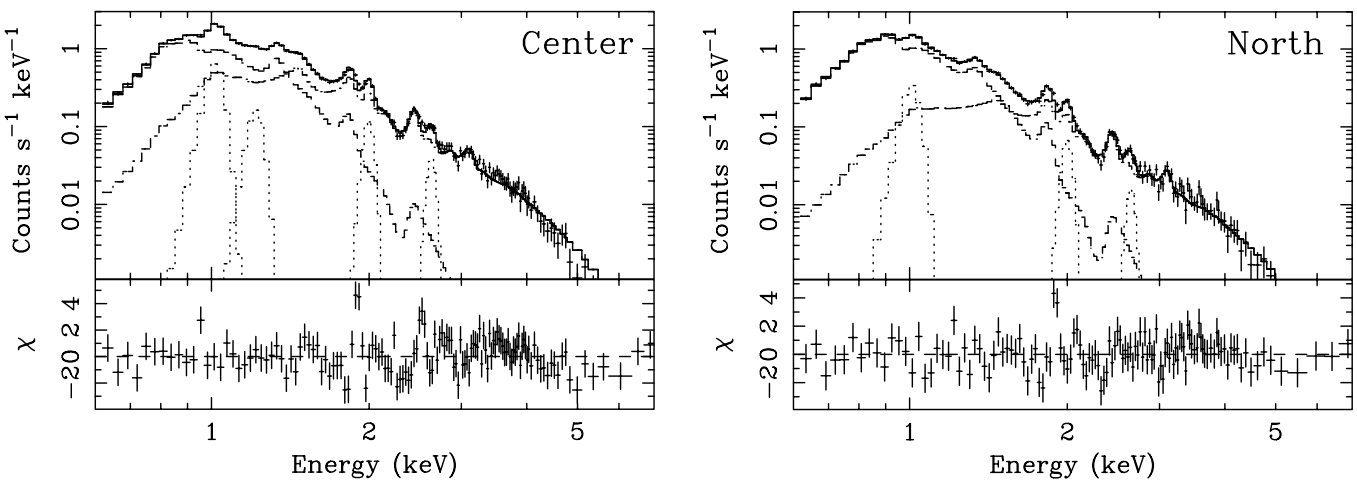

FIG. 6.—SIS spectra of the center (*left*) and north (*right*) regions with the best-fit two-plasma and Gaussian models. Dashed, dash-dotted, and dotted lines represent the 0.2 keV plasma, 1.0 keV plasma, and additional Gaussians, respectively. The bottom panels show the residuals of the fit.

TABLE 2
BEST-FIT PARAMETERS OF THE TWO-PLASMA MODEL

MODEL	PARAMETER	NORTH REGION		CENTER REGION	
		Value	90% Confidence Range	Value	90% Confidence Range
Wabs[a]	$N_H(10^{21}$ cm$^{-2})$	7.3	6.7–7.9	7.5	6.9–8.4
VGNEI (low T)	kT (keV)	0.17	015–0.19	0.18	0.16–0.21
	$n_e t$ (10^{11} cm^{-3} s)	1.0	0.7–1.5	1.0	0.7–1.5
	$\langle kT \rangle$ (keV)	0.44	0.39–0.53	0.51	0.46–0.59
	Constant factor[b]	185	117–287	48	24–87
VRAYMOND (high T)	kT (keV)	1.09	1.01–1.19	1.06	1.01–1.11
	Emission measure[c]	0.038	0.030–0.046	0.056	0.048–0.064
Abundance	O	0.03	0.02–0.04	0.07	0.05–0.10
	Ne	0.09	0.08–0.11	0.12	0.10–0.16
	Mg	0.11	0.09–0.14	0.25	0.19–0.35
	Si	0.42	0.34–0.52	0.38	0.32–0.47
	S	0.43	0.35–0.54	0.43	0.38–0.49
	Ar	0.64	0.39–0.89	0.57	0.41–0.72
	Fe	0.07	0.05–0.09	0.17	0.14–0.20
Ne x Kα	Observed energy (keV)	1.012	1.006–1.018	1.021	1.018–1.025
	Flux[d]	21	18–26	29	23–39
Ne x Kβ	Observed energy (keV)	...	...	1.223	1.215–1.231
	Flux[d]	...	...	3.1	2.3–4.1
Si XIV Kα	Observed energy (keV)	2.015	2.002–2.011	2.011	2.002–2.018
	Flux[d]	1.1	0.8–1.4	1.3	1.1–1.6
S XVI Kα	Observed energy (keV)	2.664	2.641–2.679	2.649	2.630–2.665
	Flux[d]	0.31	0.20–0.42	0.53	0.43–0.64
N/A	χ^2/dof	160/108	...	226/116	...

NOTE.—Each abundance is relative to the solar value and those of two plasma components linked together. The line width of each Gaussian profile is fixed to 0.

[a] Wabs is a model of a photoelectric absorption in XSPEC.

[b] This constant factor is the ratio of the VGNEI emission measure to the VRAYMOND emission measure in XSPEC.

[c] The unit is $4\pi d^2 \times 10^{14}$ cm^{-5}, where d is the distance to IC 443.

[d] The unit is 10^{-4} photons cm^{-2} s^{-1}.

emitted from an "overionized" 1.0 keV plasma (i.e., a plasma in which the degree of ionization is larger than that expected from the electron temperature assuming CIE).

4. DISCUSSION

4.1. *The Plasma Structure of IC 443*

ASCA observations have revealed the following new X-ray features of IC 443; (1) the X-ray softness-ratio map shows a shell-like structure that correlates with the optical filaments, implying that the hard X-ray emission is more centrally concentrated than the soft; (2) the spectra include two plasma components with temperatures of 0.2 and 1.0 keV, and the intensity ratio of the former to the latter is larger in the outer region than in the inner region.

These results suggest that IC 443 has a plasma structure that can be modeled by a central hot (1.0 keV) region surrounded by a cooler (0.2 keV) shell. The mean electron den-

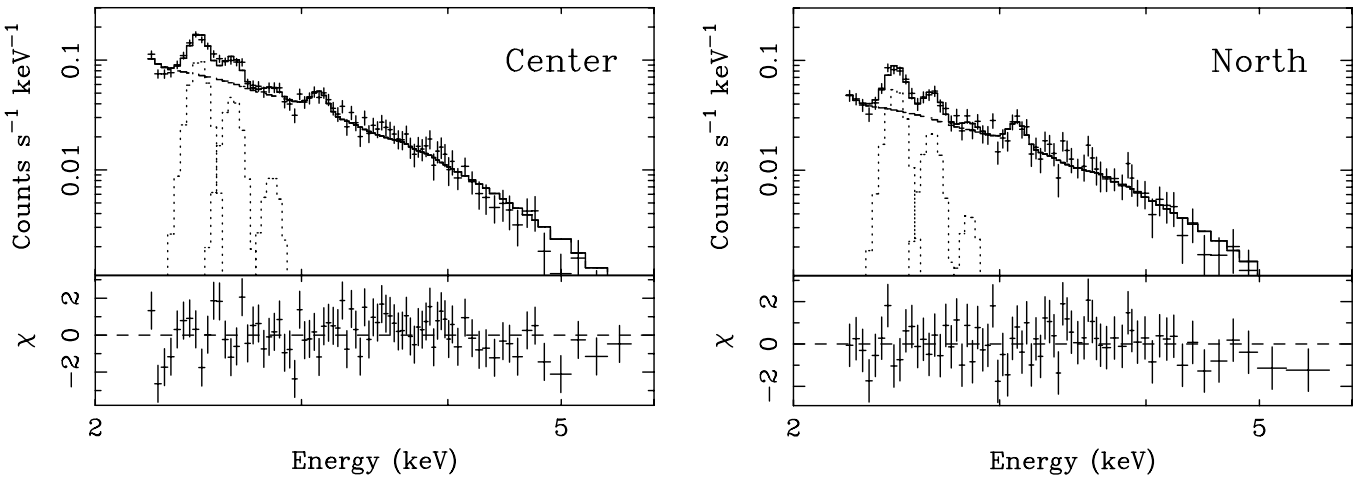

FIG. 7.—SIS spectra of the center (*left*) and north (*right*) regions with the best-fit model of Raymond-Smith (*dashed line*) and three narrow Gaussian components (*dotted lines*) with $N_H = 7.4 \times 10^{21}$ cm^{-2} at energies of 2.2–6.0 keV. The bottom panels show the residuals of the fit, and the minimum values of reduced χ^2 are 85/70 and 53/59 in the center and north, respectively.

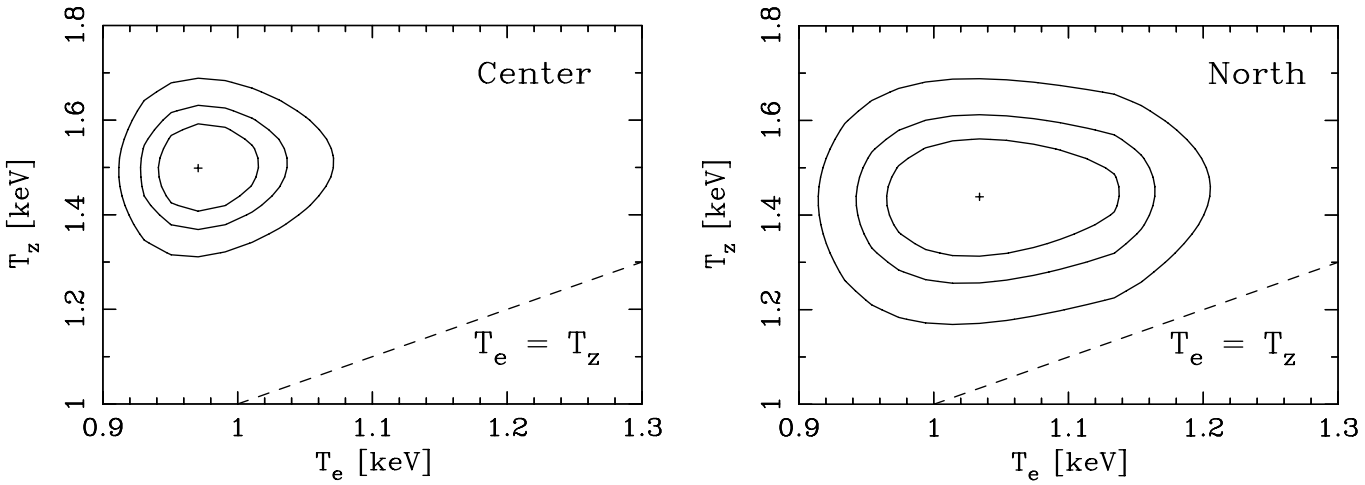

FIG. 8.—Confidence contours in the T_e (the continuum temperature)-T_z (the ionization temperature) space of the SIS spectra in the center (*left*) and north (*right*). The confidence levels are 99%, 90%, and 67%. The contours are above the dashed line, which implies that the ionization temperature is higher than the continuum temperature in each figure.

sities within these regions are estimated from the observed emission measures. The emission measure of the 1.0 keV plasma, which is estimated from the GIS spectrum of the brightest region within a 16′ radius (northeast part of IC 443, where most X-rays are emitted), is $\simeq 1.1 \times 10^{58} (d/1.5 \text{ kpc})^2 \text{ cm}^{-3}$ (d is the distance to IC 443). In contrast, that of the 0.2 keV plasma is $\simeq 5.4 \times 10^{59} (d/1.5 \text{ kpc})^2 \text{ cm}^{-3}$, more than an order of magnitude larger. To estimate the densities of the two components, we assume that the 0.2 keV plasma extends to the northeast optical shell and thus has an outer radius of $\theta_2 = 16'$. The radius of the region containing the 1.0 keV component is assumed to be $\theta_1 = 10'$, considering that the surface brightness of the 1.0 keV plasma at this radius is 50% of its maximum (from the 2.0–3.5 keV band image). The densities of the 1.0 keV plasma (n_1) and the 0.2 keV plasma (n_2) are

$$n_1 = 1.0 \left(\frac{\theta_1}{10'} \right)^{-3/2} \left(\frac{d}{1.5 \text{ kpc}} \right)^{-1/2} \text{cm}^{-3} , \quad (1)$$

$$n_2 = 4.2 \left(\frac{a^3 - 1}{3.096} \right)^{-1/2} \left(\frac{\theta_1}{10'} \right)^{-3/2} \left(\frac{d}{1.5 \text{ kpc}} \right)^{-1/2} \text{cm}^{-3} , \quad (2)$$

where $a = \theta_2/\theta_1$. The cooler exterior shell is denser than the interior; the two components appear to be near pressure equilibrium and consistent with a typical SNR predicted by the Sedov-Taylor solution, despite the fact that the X-ray image appears center-filled.

This structure is also consistent with the prediction of the conduction model for MM SNRs developed for W44 (Cox et al. 1999; Shelton et al. 1999). These authors suggest that if a remnant evolving in a fairly smooth ambient medium of moderate density with thermal conduction active in its interior reaches the phase in which radiative cooling is important, then it shows inner-hot and outer-cool regions of X-ray emission interior to the cold dense shell. IC 443 has similar characteristics to W44, including a partial H I shell, suggesting it is in the same evolutionary state.

4.2. *Formation Mechanisms of the Overionized Plasma*

In addition, we find that the Kα lines of H-like Si and S are unusually strong, indicating that the plasma in IC 443 is overionized. This is the first detection of evidence for an overionized plasma in an SNR. In SNRs, we are accustomed to consider the plasma underionized, since in a collisionally ionized, shock-heated plasma, the ionization timescale is typically large compared to the time since the bulk of the gas was shock heated. Nevertheless, conditions can (and apparently do) exist in which a shock-heated, low-density plasma can become overionized. In this section, we discuss possible formation mechanisms for such a plasma.

We can consider two possible ways to produce an overionized plasma. One is that photoionization causes heavy elements to be more highly ionized than their collisional equilibrium level. A low-density plasma does not produce sufficient radiation to photoionize the heavy elements: the plasma needs a bright external radiation source. CXOU J061705.3+222127, with a 1–5 keV flux of 2×10^{-13} ergs cm^{-2} s^{-1} (Olbert et al. 2001; Bocchino & Bykov 2001), is too faint to photoionize the 1.0 keV plasma to emit the "extra" H-like S flux of $\sim 10^{-13}$ ergs cm^{-2} s^{-1} shown in Table 2, even if it was at the center of the remnant in the past. Futhermore, there is no other evidence of such a strong source in IC 443, and it is implausible to consider that this plasma region is illuminated continuously by a hidden intense source.

The other way is that the gas cools faster than the ions can recombine. The three possible cooling mechanisms in the gas are radiation, expansion, and thermal conduction. Shelton (1998, 1999) has shown that inclusion of all three processes in hydrodynamic modeling of SNRs expanding in a very low density ISM leads to the development of an "overionized" plasma in the interior once a remnant has reached the radiative stage. The H I shell covering the eastern part of the remnant (Giovanelli & Haynes 1979) suggests that at least part of IC 443 is in the radiative stage. Below, we compare the cooling timescales of radiation, expansion, and conduction with the recombination timescale of heavy elements in the 1.0 keV plasma and show that these are consistent with the formation of an overionized plasma in IC 443.

The recombination timescale of an element of atomic number Z, which is the characteristic timescale to reach ionization equilibrium, is calculated by Masai (1994). In the

case of sulfur at a temperature of 1.0 keV, this is estimated to be

$$t_{\rm recomb} \approx \sum_{z=0}^{Z} (S_z + \alpha_z)^{-1} \simeq 9 \times 10^{11} \left(\frac{n_1}{1\ {\rm cm}^{-3}} \right)^{-1} {\rm s}\ , \quad (3)$$

where S_z and α_z represent the rate coefficients for ionization and recombination for an ion of charge z to charge $z+1$ and $z-1$, respectively. This is consistent with the expectation that collisional-ionization equilibrium is approached for the ionization timescale value $n_e t \sim 10^{12}\ {\rm cm}^{-3}\ {\rm s}$.

We estimate the cooling timescale of the 1.0 keV plasma via radiation to be

$$t_{\rm cool} = \frac{3 n_1 k T_1 V}{L_{\rm rad}} \simeq 4 \times 10^{14} \left(\frac{\theta_1}{10'} \right)^{3/2} \left(\frac{d}{1.5\ {\rm kpc}} \right)^{1/2} {\rm s}\ , \quad (4)$$

where V and $L_{\rm rad}$ are the volume and the luminosity of the 1.0 keV plasma, respectively. The cooling timescale of equation (4) is more than 2 orders of magnitude larger than the recombination timescale of equation (3).

Rapid adiabatic cooling and the resulting overionization have been discussed by Itoh & Masai (1989) for a young remnant breaking out of the circumstellar matter into a rarefied medium. However, this is not the case for IC 443, which is presumed to be in its Sedov phase (expansion of the shocked ejecta is negligible compared to the blast wave). The shock temperature decreases with blast wave expansion. Even if the effect is taken into account, it is found that the electron temperature varies as slowly as $T_e \propto t^{-2/25}$ with Coulomb collisions in the postshock region (Itoh 1978; Masai 1994). Therefore, adiabatic expansion is unlikely to work, since the timescale is much longer than the recombination timescale.

We next calculate the energy transport rate by thermal conduction from the 1.0 keV interior to the 0.2 keV outer region. We assume a temperature gradient scale length, $l_T \equiv (\mathrm{grad} \ln T)^{-1}$, of $(1\text{–}2) \times 10^{19}$ cm, the distance from the approximate boundary between the 1.0 and 0.2 keV components to the edge of the remnant. This distance is much longer than the mean free path of electrons $\lambda_e \approx 10^{18} (T_e/10^7\ {\rm K})^2 (n_e/1\ {\rm cm}^{-3})^{-1}$ cm. The total flow of heat to the outer plasma is estimated to be $2 \times 10^{38} (l_T/10^{19}\ {\rm cm})^{-1} (\theta_1/10')^2 (d/1.5\ {\rm kpc})^2$ ergs s^{-1}. The energy loss via radiation in the 0.2 keV plasma is 7×10^{37} ergs s^{-1} from the observed emission measure, comparable to the heat flow. In this circumstance, thermal conduction equilibrates the temperatures of the two components on the conduction timescale,

$$t_{\rm cond} \equiv -\left(\frac{d \ln T_e}{dt} \right)^{-1} \approx \frac{n_e l_T^2 k}{\kappa}$$
$$\simeq 2 \times 10^{11} \left(\frac{n_1}{1\ {\rm cm}^{-3}} \right) \left(\frac{l_T}{10^{19}\ {\rm cm}} \right)^2$$
$$\times \left(\frac{k T_1}{1.0\ {\rm keV}} \right)^{-5/2} \left(\frac{\ln \Lambda}{32.2} \right) {\rm s}\ , \quad (5)$$

where $\ln \Lambda$ is the Coulomb logarithm. The gas in the 1.0 keV plasma cools on the timescale given by equation (5). This timescale is smaller than the recombination timescale and is comparable to it even with $l_T = 2 \times 10^{19}$ cm. This indicates that the strong gas cooling via conduction makes T_e lower than T_z. While the presence of a magnetic field will in principle reduce the heat flux, we ignore its effect, since the magnetic field is expected to be negligibly small in mature SNRs. We conclude from this argument that it is entirely possible in IC 443 and similar SNRs for the interior gas to be an overionized, recombining plasma.

Assuming both T_z and T_e are e-folding with their characteristic timescales, we can approximately estimate the age of the 1.0 keV plasma ($t_{\rm age}$) by the equation

$$\frac{T_z}{T_e} \approx \frac{\exp(-t_{\rm age}/t_{\rm recomb})}{\exp(-t_{\rm age}/t_{\rm cond})} \sim 1.5\ , \quad (6)$$

to be $(0.3\text{–}1) \times 10^4$ yr. This age is younger than that estimated by Chevalier (1999). It at least indicates that the 1.0 keV plasma is younger than $t_{\rm recomb} \approx 3 \times 10^4$ yr; if this plasma is older than the age represented by the recombination timescale, we would expect T_z to be comparable to T_e.

Evidence of overionization has not been detected in any other SNR. We consider our detection in IC 443 to be plausible for the following reasons: (1) The interior of IC 443 was shocked long ago and has had no subsequent source of heating or ionization and thus should be much nearer ionization equilibrium than newly shocked gas near the rim or in young SNRs. (2) IC 443 has an interior plasma hot enough to give rise to strong thermal conduction. (3) *ASCA* SIS is the first detector with sufficient energy resolution to cleanly resolve the H-like and He-like lines of S from each other. (4) The signal-to-noise ratio in the spectra is sufficiently high [$(4\text{–}5) \times 10^4$ counts in each region] for T_z and T_e to be inferred with small errors. It should be noted, however, that no evidence of overionization is detected in W44, despite it having similar properties and comparable quality of *ASCA* spectra. The difference between the two remnants merits further investigation.

5. CONCLUSION

We have discovered a shell-like structure in the softness-ratio map and two distinct (0.2 and 1.0 keV) plasma components in IC 443. Using these results and the emission measures of the two components, we suggest that IC 443 has a plasma structure consisting of a central hot region surrounded by an envelope of a cool and denser plasma: that is, the typical structure of an SNR predicted by the Sedov-Taylor solution. In addition, we have detected strong line emission from H-like Ne, Si, and S. The line intensity ratio of H-like to He-like Kα of S requires a temperature of 1.5 keV, which is significantly higher than the continuum temperature of 1.0 keV. The same can be concluded for Si. Therefore, we suggest that the 1.0 keV plasma is "overionized."

In order to produce an overionized thermal plasma, the gas cooling rate must be higher than the recombination rate of ions. Strong cooling due to thermal conduction from the hot (1.0 keV) remnant center to the cooler (0.2 keV) exterior could cause this.

IC 443 is the first SNR in which evidence for overionization has been found. The process of thermal conduction should arise in all SNRs. Therefore, we expect that observations of other evolved SNRs (such as mixed-morphology types) should detect further evidence of overionized plasma. The apparent absence of overionized gas in the similar remnant W44 suggests that the interior plasma in other remnants may evolve differently from that in IC 443.

We thank Yasunobu Uchiyama for his thoughtful comments and suggestions. The Digitized Sky Survey was produced at the Space Telescope Science Institute under US Government grant NAG W-2166. The images of these surveys are based on photographic data obtained using the Oschin Schmidt Telescope on Palomar Mountain and the UK Schmidt Telescope. The plates were processed into the present compressed form with the permission of these institutions.

REFERENCES

Anders, E., & Grevesse, N. 1989, Geochim. Cosmochim. Acta, 53, 197
Asaoka, I., & Aschenbach, B. 1994, A&A, 284, 573
Bocchino, F., & Bykov, A. M. 2000, A&A, 362, L29
———. 2001, A&A, 376, 248
Borkowski, K. J. 2000, Rev. Mexicana Astron. Astrofis., 9, 288
Chevalier, R. A. 1999, ApJ, 511, 798
Cornett, R. H., Chin, G., & Knapp, G. R. 1977, A&A, 54, 889
Cox, D. P., Shelton, R. L., Maciejewski, W., Smith, R. K., Plewa, T., Pawl, A., & Różyczka, M. 1999, ApJ, 524, 179
Ezuka, H., & Ishida, M. 1999, ApJS, 120, 277
Fesen, R. A. 1984, ApJ, 281, 658
Giovanelli, R., & Haynes, M. P. 1979, ApJ, 230, 404
Hartman, R. C., et al. 1999, ApJS, 123, 79
Holt, S. S., Gotthelf, E. V., Tsumeni, H., & Negoro, H. 1994, PASJ, 46, L151
Itoh, H. 1978, PASJ, 30, 489
Itoh, H., & Masai, K. 1989, MNRAS, 236, 885
Keohane, J. W., Petre, R., Gotthelf, E. V., Ozaki, M., & Koyama, K. 1997, ApJ, 484, 350
Masai, K. 1994, ApJ, 437, 770
Mewe, R., Gronenschild, E. H. B. M., & van den Oord, G. H. J. 1985, A&AS, 62, 197
Miyata, E., Tsunemi, H., Pisarski, R., & Kissel, S. E. 1994, PASJ, 46, L101
Olbert, C. M., Clearfield, C. R., Williams, N. E., Keohane, J. W., & Frail, D. A. 2001, ApJ, 554, L205
Petre, R., Szymkowiak, A. E., Seward, F. D., & Willingale, R. 1988, ApJ, 335, 215
Raymond, J. C., & Smith, B. W. 1977, ApJS, 35, 419
Rho, J.-H., & Petre, R. 1998, ApJ, 503, L167
Shelton, R. L. 1998, ApJ, 504, 785
———. 1999, ApJ, 521, 217
Shelton, R. L., Cox, D. P., Maciejewski, W., Smith, R. K., Plewa, T., Pawl, A., & Różyczka, M. 1999, ApJ, 524, 192
Tanaka, Y., Inoue, H., & Holt, S. S. 1994, PASJ, 46, L37
Wang, Z. R., Asaoka, I., Hayakawa, S., & Koyama, K. 1992, PASJ, 44, 303
White, R. L., & Long, K. S. 1991, ApJ, 373, 543